Structure and phase transition in the $(C_5H_{10}NH_2)SbCl_6 \cdot (C_5H_{10}NH_2)Cl$ crystal

2000 J. Phys.: Condens. Matter 12 1143

(http://iopscience.iop.org/0953-8984/12/7/301)

J. Phys.: Condens. Matter **12** (2000) 1143–1159. Printed in the UK PII: S0953-8984(00)05979-8

Structure and phase transition in the $(C_5H_{10}NH_2)SbCl_6 \cdot (C_5H_{10}NH_2)Cl$ crystal

B Bednarska-Bolek†, A Pietraszko‡, R Jakubas†, G Bator† and B Kosturek§

† Faculty of Chemistry, University of Wroclaw, F Joliot Curie 14, 50-383 Wroclaw, Poland
‡ Institute of Low Temperature and Structure Research of the Polish Academy of Science, Okólna 2, 50-422 Wroclaw, Poland
§ Institute of Experimental Physics, University of Wroclaw, 9 Max Born Square, 50-204 Wroclaw, Poland

Received 13 July 1999, in final form 16 November 1999

Abstract. Differential scanning calorimetry, dilatometric, dielectric dispersion and linear birefringence measurements have been used to study the phase transition at 202 K in the $(C_5H_{10}NH_2)SbCl_6 \cdot (C_5H_{10}NH_2)Cl$ crystal. The x-ray studies show that at room temperature it crystallizes in the orthorhombic symmetry (space group $Pccn$), whereas below 202 K the structure changes its symmetry to monoclinic ($P2_1/c$). The mechanism of the phase transition is connected both with the disordering of the piperidinium cations and the essential change in the NH...Cl hydrogen bond system. The title crystal exhibits the ferroelastic domain structure in the monoclinic phase.

1. Introduction

Simple salts of alkylammonium, $(CH_3)_nNH_{4-n}^+$, cations and inorganic anions such as ClO_4^- [1], BF_4^- [2], NO_3^- [3], PF_6^- [4] are reported to form a mesophase of the CsCl-type cubic structure. In these phases both cations and anions may perform isotropic rotation. Such a dynamical disorder is characteristic of the so called 'ionic plastic phase'. In searching for new materials with similar mesophase we extended the studies to the alkylammonium halogenoantimonates(V). Up to now four salts belonging to this family have been studied: $[P(CH_3)_4]SbCl_6$ [5], $[C(NH_2)_3]SbCl_6$ [6] and $[N(CH_3)_4]SbCl_6$ and $[N(CH_3)_4]SbCl_6$ [7]. The structure of these salts appeared to be quite simple. It consists of the isolated $SbCl_6^-$ anions and organic cations. In the high temperature phases of guanidinium and tetramethylphosphonium halogenoantimonates(V) the organic cations revealed isotropic rotations, but the ionic plastic phases were not directly evidenced. On the other hand these two salts, within ordered low temperature phases, appeared to be a new ferroic material showing ferroelasticity. The ferroic properties were suggested to be connected with the organic cation dynamics. The incorporation of cyclic ammonium cations like piperidinium, $C_5H_{10}NH_2^+$, into the crystal lattice of chloroantiomonates(V), may create salts exhibiting potentially the ferroelasticity or ionic plastic phases. In the present work we report x-ray, differential scanning calorimetry, dielectric dispersion and birefringence studies of a new piperidinium salt, $(C_5H_{10}NH_2)SbCl_6 \cdot (C_5H_{10}NH_2)Cl$ (abbreviated PCAPC). An attempt is made to propose the mechanism of the para–ferroelastic phase transition at 202 K.

0953-8984/00/071143+17$30.00

Table 1. Crystal data and structure refinement for PCAPC.

	293 K	185 K
Identification code	$(C_5H_{10}NH_2)SbCl_6 \cdot (C_5H_{10}NH_2)Cl$	
Empirical formula	$C_{10}H_{24}C_{17}N_2Sb$	
Formula weight	542.21	
Temperature	293(2) K	185(2) K
Wavelength	0.710 73 Å	0.710 73 Å
Crystal system, space group	Orthorhombic, $Pccn$	Monoclinic, $P2_1/c$
Unit cell dimensions	$a = 12.525(3)$ Å $\alpha = 90^\circ$	$a = 12.427(2)$ Å $\alpha = 90^\circ$
	$b = 17.871(4)$ Å $\beta = 90^\circ$	$b = 17.601(4)$ Å $\beta = 90^\circ$
	$c = 19.220(4)$ Å $\gamma = 90^\circ$	$c = 19.172(4)$ Å $\gamma = 90^\circ$
Volume	4302.1(17) Å^3	4193.4(15) Å^3
Z, calculated density	8, 1.674 Mg m^{-3}	8, 1.718 Mg m^{-3}
Absorption coefficient	2.145 mm^{-1}	2.201 mm^{-1}
$F(000)$	2144	2144
Crystal size	$0.24 \times 0.32 \times 0.28$ mm^3	$0.24 \times 0.34 \times 0.28$ mm^3
θ-range for data collection	4.56 to 23.26°	4.54 to 23.82°
Limiting indices	$-13 \leqslant h \leqslant 13$, $-19 \leqslant k \leqslant 19$, $-21 \leqslant l \leqslant 11$	$-13 \leqslant h \leqslant 13$, $-19 \leqslant k \leqslant 19$, $-15 \leqslant l \leqslant 21$
Reflections collected/unique	15023/3012 (R(int) = 0.0490)	17858/5874 (R(int) = 0.0442)
Completeness to theta = 23.26	97.5%	91.3%
Refinement method	Full-matrix least squares on F^2	Full-matrix least squares on F^2
Data/restraints/parameters	3012/0/298	5874/0/536
Goodness of fit on F^2	1.250	1.155
Final R indices ($I > 2\sigma(I)$)	$R_1 = 0.0486$, $wR_2 = 0.1055$	$R_1 = 0.0534$, $wR_2 = 0.1266$
R indices (all data)	$R_1 = 0.0603$, $wR_2 = 0.1192$	$R_1 = 0.0640$, $wR_2 = 0.1412$
Extinction coefficient	0.000 25(12)	0.000 53(8)
Largest diff. peak and hole	0.818 and −0.847 e Å^{-3}	1.432 and −1.287 e Å^{-3}

2. Experimental details

$(C_5H_{10}NH_2)SbCl_6 \cdot (C_5H_{10}NH_2)Cl$ was prepared by reacting $(C_5H_{10}NH_2)Cl$ and $SbCl_5$ in concentrated hydrochloric acid. The resulting white solid was re-crystallized twice from an ethanol solution. The single crystals of PCAPC were grown from the solution by the controlled solvent evaporation technique.

Differential scanning calorimetry (DSC) measurements were carried out using a Perkin–Elmer DSC-7 calorimeter. The DSC measurements were performed with the cooling/heating rates ranging from 3 K min^{-1} to 20 K min^{-1}.

The linear thermal expansion was measured using a Perkin–Elmer TMA-7 thermomechanical analyser. The samples used in the measurements were prepared in the form of rods of dimensions $3 \times 3 \times 6$ mm^3. The dilatometric measurements were performed during heating and cooling runs at a rate of 1.5 K min^{-1}. The accuracy of the thermal expansion determination was about 5%.

The complex electric permittivity, ε^*, was measured using the HP 4284A and HP 4285A precision LCR meters in the frequency range between 1 kHz and 30 MHz and in the temperature region 100–300 K. The measurements were performed with a cooling/heating rate of 0.5 K min^{-1} in the vicinity of the phase transitions and 2 K min^{-1}, elsewhere. Plates with the typical dimensions of $5 \times 5 \times 1$ mm^3 were cut perpendicularly to all crystallographic axes and they were silver painted. The overall error for the real and imaginary part of the complex electric permittivity was less than 5%.

The following optical methods were applied for detection of the phase transition and description of the resulting phases: polarized microscopy observations monitored by CCD camera, measurements of the absolute value of the linear birefringence and determination of the optical indicatrix position inside ferroelastic domains using the Ehringhaus compensator. A 1 mW He–Ne laser served as a light source ($\lambda = 632.8$ nm). The accuracy achieved for the birefringence change measurements was 10^{-6}. The cooling and heating rates were 0.5 K min^{-1} (0.2 K min^{-1} in the phase transition regions).

Single crystal x-ray intensity data were collected at room temperature (293 K) in the orthorhombic phase and at 185 K in the monoclinic phase. Data were obtained with Mo Kα radiation ($\lambda = 0.710\,73$ Å) by using the four circle x-ray diffractometer KM4-CCD (KUMA Diffraction Company). The CCD detector of aperture diameter of 92 mm was used to collect the data. The technical parameters of the CCD detector were the following: 1024×1024 pixels, 24 μm^2 pixel size on taper; Gadox scintillator absorption 65–74%; 10 e$^-$-overall noise rms; 0.3 e$^-$/pixel s^{-1} dark current; 260×10^3 e$^-$/pixel s^{-1} signal saturation, 3.8 s (2×2 bining) read-out time including data transfer to main computer. The distance between the samples and the detector was 70.25 mm. The data were collected in four runs at 120°ω angle using a step $\Delta\omega = 0.5^\circ$ and 30 s exposures for one image. The sample was mounted on a glass fibre and cooled to 185 K by using liquid nitrogen (Oxford Cryo-system). Data of experimental conditions at 293 and 185 K are presented in table 1.

The temperature dependence of lattice parameters was measured in the temperature range from 95 to 300 K. Measurements were carried out using the CCD detector and special image processing. The images at each temperature point were recorded with oscillation $\Delta\omega = 1^\circ$ for ten runs in two positions of $+2\Theta$ and -2Θ angle for several different κ and ϕ angles. The lattice parameters were calculated from 140–160 reflections with accuracy of $\Delta a/a = 10^{-4}$.

3. Results

3.1. X-ray data

At room temperature the systematic absences pointed out to the space group $Pccn$. The symmetry below the transition point (202 K) changed to the space group $P2_1/c$. The structure was solved by the Patterson method using the SHELXS-97 program and accomplished by using difference Fourier methods. The positions of hydrogen atoms were determined from difference Fourier maps. Refinement was carried out using SHELX-97 [8]. The larger value of the final R factor for the monoclinic phase than for the orthorhombic phase is a result of partial twinning of crystals. During the refinement of the structure of the low temperature phase the corrections for the twinning were applied.

The projections along the c- and a-axes of the crystal structure at room temperature are shown in figures 1 and 2, respectively. Isolated $SbCl_6^-$ octahedra, separated from one another by two crystallographically independent piperidinium cations and an isolated chlorine anion, are the most prominent feature of the orthorhombic structure. The N atoms of the piperidinium cations are connected by the hydrogen bonds to the isolated Cl^- ions. In the monoclinic low temperature phase at 185 K the asymmetric unit consists of four crystallographically non-equivalent piperidinium cations. In both phases the $SbCl_6$ octahedra are ordered, but one of two independent $C_5H_{10}NH_2^+$ cations appeared to be disordered in the orthorhombic phase. The details of data collection and refinement at 293 and 185 K are given in tables 2 and 3.

In the orthorhombic phase the piperidinium groups form a spiral chain parallel to the c-axis, with the Cl atom arrangement inside the channel of this chain. One of the two piperidinium cations, being ordered, possesses a chair conformation. The second one is disordered, for

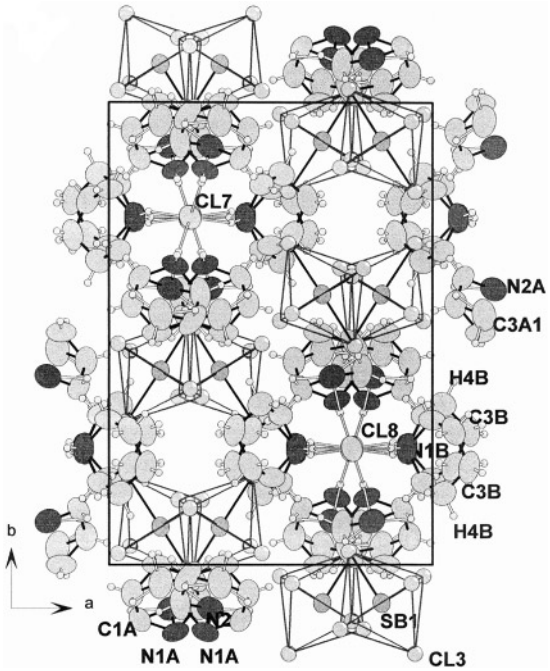

Figure 1. Projection of the crystal structure of PCAPC on the *a*–*b*-plane at room temperature (293 K).

which both N(1A) and C(3A) atoms are distributed between two positions (the refined site occupation factors equal to 0.61 for N(1A) and 0.61 for C(3A)). The hydrogen bonds of the cation–Cl–cation chain for two temperatures are illustrated in figures 3(a) and (b). The distances and angles for the N–H . . . Cl hydrogen bonds are presented in table 3.

The phase transition from orthorhombic phase to monoclinic one at 202 K is partially a result of the ordering of the piperidinium groups. In the low temperature phase the crystal structure consists of two crystallographically independent $SbCl_6$ units and four ordered piperidinium groups possessing a chair conformation. The result of this arrangement of the piperidinium cations in the monoclinic phase is the separation of the chains into isolated groups of the cation–Cl–cation type (figure 3(b)). The hydrogen bonds in the low temperature phase for isolated cation–Cl–cation groups are significantly shorter than those found in the orthorhombic phase.

3.2. Differential scanning calorimetry and dilatometric measurements

The DSC curves during cooling/heating scans are presented in figure 4(a). In the low temperature region one well reversible heat anomaly is revealed at about 203 ± 1 K. The shape of the heat anomaly and relatively small thermal hysteresis (extrapolated to the scanning rate of 0 K min^{-1}, $\Delta T < 0.2$ K) clearly indicate the continuous nature of the phase transition.

Figure 4(b) shows the linear thermal expansion of the PCAPC crystal on cooling along three crystallographic directions (the notation of the axes is according to the orientation of the crystal in the orthorhombic phase). A distinct thermal anomaly in dilation at 202 ± 1 K confirms the presence of the phase transition. Along the *a*-axis the anomaly is hardly visible whereas for the *b*-axis a distinct change in the slope of thermal dilation is observed at the phase

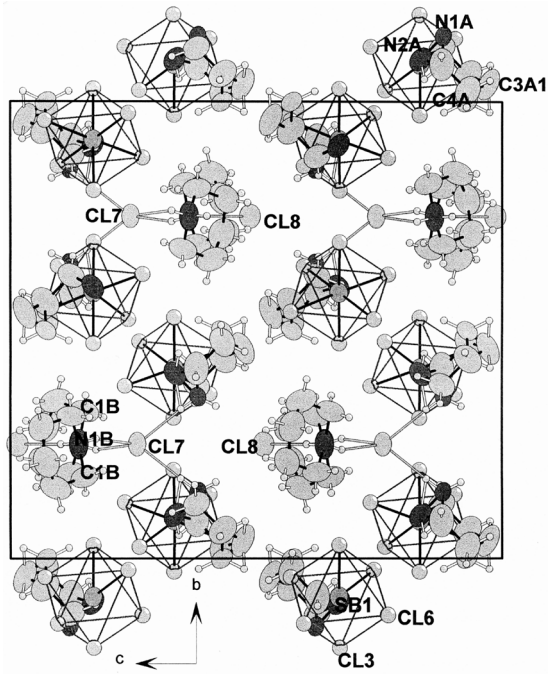

Figure 2. Projection of the crystal structure of PCAPC on the *c*–*b*-plane at room temperature (293 K).

transition point. For the *c*-direction below 202 K one can observe a change in the sign of thermal expansion coefficient. Along the *a*- and *b*-axes the crystal expands practically linearly with comparable thermal expansion coefficients both above and below T_c. The mean value of the thermal expansion coefficient (the mean value of α is defined as $(L_1 - L_2)/L_{(300\ K)}(T_1 - T_2)$) is equal to about $\bar{\alpha}_{a,b} \approx 8 \times 10^{-5}\ \mathrm{K}^{-1}$. For the *c*-axis this coefficient is distinctly smaller and amounts to about $3 \times 10^{-5}\ \mathrm{K}^{-1}$ in the paraelastic phase.

The temperature dependences of the lattice parameters of the PCAPC crystals obtained from the x-ray measurements are illustrated in figure 5. It is seen that the temperature characteristic of these parameters is qualitatively similar to that found by the linear thermal expansion measurements. We should notice that the β monoclinic angle reveals a continuous change in the slope around 202 K. This clearly supports the change of symmetry of crystals from orthorhombic to monoclinic.

3.3. Dielectric studies

From the crystallographic results it is known that in the PCAPC crystal one of two independent organic cations is disordered in the high temperature phase. If this disorder is dynamical the dielectric dispersion and absorption should be observed in the orthorhombic phase. This is a result of the fact that motion of the piperidinium cation (simultaneous flip-flop of the N(1A) and C(3A) atoms) should lead to an increase of the polarization of the crystal. This model of the cationic disorder suggests also the possible anisotropy of the dielectric properties.

Figure 6 presents the temperature dependence of the complex electric permittivity, $\varepsilon^* = \varepsilon' - \mathrm{i}\varepsilon''$, measured at 10 kHz along three crystallographic directions. It is seen that no difference in the value of both ε' and ε'', within an experimental error is observed along

Table 2. Atomic coordinates ($\times 10^4$) and equivalent isotropic displacement parameters (Å$^2 \times 10^3$). $U(eq)$ is defined as one third of the trace of the orthogonalized U_{ij} tensor.

	293 K					185 K			
	x	*y*	*z*	*U* (eq)		*x*	*y*	*z*	*U* (eq)
Sb(1)	1584(1)	832(1)	1673(1)	53(1)	Sb(1)	1579(1)	804(1)	1681(1)	30(1)
Cl(1)	283(1)	251(1)	2389(1)	85(1)	Cl(1A)	2583(2)	−349(1)	1615(1)	54(1)
Cl(2)	2594(1)	−290(1)	1680(1)	100(1)	Cl(2A)	547(2)	1926(1)	1778(1)	52(1)
Cl(3)	548(1)	1929(1)	1689(1)	99(1)	Cl(3A)	625(2)	467(1)	671(1)	50(1)
Cl(4)	646(1)	410(1)	692(1)	86(1)	Cl(4A)	256(1)	163(1)	2364(1)	50(1)
Cl(5)	2861(1)	1403(1)	957(1)	94(1)	Cl(5A)	2515(2)	1102(1)	2714(1)	63(1)
Cl(6)	2506(1)	1224(1)	2677(1)	112(1)	Cl(6A)	2882(2)	1428(1)	1005(1)	53(1)
Cl(7)	−2500	2500	2432(1)	72(1)	Sb(2)	6606(1)	9174(1)	3273(1)	30(1)
Cl(8)	2500	−2500	139(1)	80(1)	Cl(1B)	2097(2)	3569(1)	1030(1)	49(1)
N(1A)	7961(6)	3539(3)	1201(3)	72(2)	Cl(2B)	7589(2)	10 326(1)	3323(1)	55(1)
C(1A)	−945(4)	3806(3)	1229(3)	93(2)	Cl(3B)	5291(2)	9784(1)	2573(1)	49(1)
C(2A)	5714(5)	623(4)	697(4)	108(2)	Cl(4B)	7582(2)	8833(1)	2255(1)	54(1)
C(3A)	3525(9)	0(5)	−711(5)	90(3)	Cl(5B)	4399(2)	3036(1)	1805(1)	53(1)
C(4A)	2422(5)	−255(4)	−701(4)	121(2)	Cl(6B)	4379(2)	4519(1)	719(1)	49(1)
C(5A)	7816(5)	837(4)	1231(4)	113(3)	Cl(7)	7489(2)	2550(1)	2417(1)	40(1)
C(3A1)	6589(13)	392(11)	285(9)	112(6)	Cl(8)	2546(2)	−2497(2)	199(1)	46(1)
N(2A)	6886(11)	954(7)	1667(6)	91(4)	N(1A)	−783(4)	2393(3)	3593(3)	41(2)
N(1B)	9206(3)	2490(3)	3619(2)	86(1)	C(1A)	310(6)	−1841(4)	1529(4)	47(2)
C(1B)	5291(5)	1780(3)	3496(4)	98(2)	C(2A)	257(6)	1590(4)	−874(5)	62(3)
C(2B)	330(5)	1551(4)	−910(4)	117(3)	C(3A)	8897(6)	7834(5)	643(4)	59(2)
C(3B)	3871(5)	2111(4)	4281(4)	112(2)	C(4A)	593(6)	2935(5)	−558(4)	54(2)
C(4B)	4357(5)	2123(4)	−619(3)	103(2)	C(5A)	18(6)	1786(4)	3788(4)	45(2)
C(5B)	5021(5)	1889(3)	−1222(4)	103(2)	N(1B)	5729(4)	2565(3)	3598(3)	39(2)
					C(1B)	5296(6)	11 801(4)	3423(4)	50(2)
					C(2B)	460(6)	3510(4)	−969(4)	53(2)
					C(3B)	3825(6)	2136(5)	4292(4)	56(2)
					C(4B)	4267(7)	2173(4)	−583(4)	48(2)
					C(5B)	5129(7)	8106(4)	1198(4)	51(2)
					C(3C)	6522(6)	10 019(4)	668(4)	48(2)
					C(1C)	5911(6)	11 219(4)	1184(4)	58(2)
					C(2C)	5737(6)	665(4)	601(4)	52(2)
					N(1C)	7028(5)	1513(3)	1167(3)	45(1)
					C(4C)	2356(6)	−306(4)	−679(4)	59(2)
					C(5C)	−2188(6)	869(5)	1259(4)	59(3)
					C(3D)	1619(7)	−411(5)	4755(4)	62(2)
					C(1D)	924(6)	−1184(5)	3777(4)	58(2)
					C(2D)	−660(6)	4407(4)	724(4)	50(2)
					N(1D)	8099(5)	4073(3)	1671(3)	49(2)
					C(4D)	2617	5203(6)	−683(4)	65(3)
					C(5D)	7137(6)	4202(4)	1201(4)	46(2)

the *a*- and *c*-axes. On the other hand a remarkable enlargement of ε' ($\sim$18 units) at room temperature along the *b*-axis is observed. Simultaneously the temperature dependence of ε'' measured along the same direction (a peak of dielectric losses) undoubtedly indicates a dielectric relaxational process. This implies that the electric permittivity measured at 10 kHz is not a static one. Nevertheless, a significant dip in the ε'_b–temperature curve at about 202 K confirms the presence of a structural phase transition. The relatively large magnitude of the

Table 3. Selected bond lengths [Å] and angles [°].

	293 K		185 K
Sb(1)–Cl(5)	2.3451(14)	Sb(1)–Cl(6A)	2.345(2)
Sb(1)–Cl(4)	2.3464(14)	Sb(1)–Cl(3A)	2.3480(18)
Sb(1)–Cl(3)	2.3509(15)	Sb(1)–Cl(5A)	2.3579(19)
Sb(1)–Cl(6)	2.3551(16)	Sb(1)–Cl(2A)	2.36615(18)
Sb(1)–Cl(2)	2.3705(15)	Sb(1)–Cl(1A)	2.3863(18)
Sb(1)–Cl(1)	2.3714(13)	Sb(1)–Cl(4A)	2.3879(19)
Cl(7)–H(0A1) No 1	2.22(4)	Sb(2)–Cl(1B) No 1	2.3498(19)
Cl(7)–H(0A1) No 2	2.22(4)	Sb(2)–Cl(6B) No 1	2.3643(19)
Cl(7)–H(0B1) No 2	2.27(4)	Sb(2)–Cl(5B) No 1	2.3654(19)
Cl(7)–H(0B1) No 1	2.27(4)	Sb(2)–Cl(2B)	2.3698(19)
Cl(7)–N(1A) No 1	3.062(6)	Sb(2)–Cl(3B)	2.3728(19)
Cl(7)–N(1A) No 2	3.06296)	Sb(2)–Cl(4B)	2.375(2)
Cl(7)–N(1B) No 2	3.126(4)	Cl(7)–H(1D1)	2.00(7)
Cl(7)–N(1B) No 1	3.126(4)	Cl(7)–H(1A1) No 2	2.11(4)
Cl(8)–H(0B2) No 3	2.27(5)	Cl(2)–H(1B1)	2.32(6)
Cl(8)–H(0B2) No 4	2.27(5)	Cl(7)–N(1C)	3.066(6)
Cl(8)–H(0A2) No 5	2.44(4)	Cl(7)–N(1A) No 2	3.128(6)
Cl(8)–H(0A2) No 6	2.44(4)	Cl(7)–N(1D)	3.132(6)
Cl(8)–N(1B) No 3	3.203(4)	Cl(7)–N(1B)	3.146(6)
Cl(8)–N(1B) No 4	3.203(4)	Cl(8)–H(1B2) No 3	2.03(6)
Cl(8)–N(1A) No 5	3.228(6)	Cl(8)–H(1C1) No 4	2.10(12)
Cl(8)–N(1A) No 6	3.228(6)	Cl(8)–N(1B) No 3	3.152(6)
N(1A)–N(2A) No 7	1.288(13)	Cl(8)–N(1C) No 4	3.184(6)
N(1A)–C(1A) No 8	1.452(9)	Cl(8)–N(1A) No 5	3.192(6)
N(1A)–C(5A) No 7	1.481(9)	N(1A)–H(1A1)	0.70(4)
C(1A)–C(2A) No 1	1.473(9)	N(1A)–H(1A2)	1.17(4)
C(2A)–C(3A1)	1.413918)	N(1A)–C(1A) No 6	1.490(9)
C(2A)–C(3A) No 5	1.464911)	N(1A)–C(5A)	1.507(8)
C(3A)–C(3A1) No 5	1.09(2)	C(1A)–C(2A) No 7	1.506(11)
C(3A)–C(4A)	1.455(12)	C(2A)–C(3A) No 8	1.527(11)
C(4A)–C(5A) No 5	1.485(10)	C(3A)–C(4A) No 8	1.502(12)
C(4A)–C(3A1) No 5	1.494(18)	C(4A)–C(5A) No 9	1.525(10)
C(5A)–N(2A)	1.450(14)	N(1B)–H(1B1)	0.84(6)
N(2A)–C(1A) No 1	1.511(14)	N(1B)–H(1B2)	1.17(6)
N(1B)–C(1B) No 7	1.468	N(1B)–C(5B) No 3	1.482(9)
N(1B)–C(5B) No 9	1.478	N(1B)–C(1B) No 10	1.486(9)
C(1B)–C(2B) No 10	1.441(10)	C(1B)–C(2B) No 11	1.511(11)
C(2B)–C(3B) No 11	1.462(9)	C(2B)–C(3B) No 9	1.500(11)
C(3B)–C(4B) No 12	1.512(9)	C(3B)–C(4B) No 12	1.517(11)
C(4B)–C(5B)	1.488	C(4B)–C(5B) No 8	1.482(10)
		C(3C)–C(4C) No 8	1.483(11)
N(1A)–H(0A1)–Cl(7) No 8	177(4)	C(3C)–C(2C) No 13	1.504(10)
N(2A) No 7–H(0A1)–Cl(7) No 8	177(4)	C(1C)–C(2C) No 13	1.499(11)
N(1A)–H(0A2)–Cl(8) No 5	168(4)	N(1C)–H(1C2)	0.75(8)
N(2A) No 7–H(0A2)–Cl(8) No 5	176(2)	N(1C)–H(1C1)	1.20(12)
N(1B)–H(0B1)–Cl(7) No 8	161(3)	N(1C)–C(1C) No 10	1.482(9)
N(1B)–H(0B2)–Cl(8) No 13	179(5)	N(1C)–C(5C) No 2	1.506(10)
Symmetry transformations used		C(5C)–C(4C) No 7	1.503(11)
to generate equivalent atoms for:		C(3D)–C(4D) No 12	1.542(12)
Pccn space groups	$P2(1)/c$	C(3D)–C(2D) No 5	1.539(11)
No 1 $-x+1/2, -y+1/2, z$	No 1 $-x+1, y+1/2, -z+1/2$	C(1D)–C(2D) No 5	1.451(11)

Table 3. (Continued)

	293 K		185 K
No 2 $x-1, y, z$	No 2 $x+1, y, z$	N(1D)–H(1D1)	1.24(7)
No 3 $x-1/2, -y, -z+1/2$	No 3 $-x+1, y-1/2, -z+1/2$	N(1D)–C(5D)	1.514(10)
No 4 $-x+1, y-1/2, -z+1/2$	No 4 $-x+1, -y, -z$	N(1D)–C(1D) No 1	1.554(10)
No 5 $-x+1, -y, -z$	No 5 $-x, y-1/2, -z+1/2$	N(1D)–H(1D2)	1.66(13)
No 6 $x-1/2, y-1/2, -z$	No 6 $-x, y+1/2, -z+1/2$	C(4D)–C(5D) No 8	1.476(11)
No 7 $-x+3/2, -y+1/2, z$	No 7 $-x, -y, -z$		
No 8 $x+1, y, z$	No 8 $-x+1, -y+1, -z$	N(1A)–H(1A2)–Cl(7) No 14	144(3)
No 9 $-x+3/2, y, z+1/2$	No 9 $x, -y+1/2, z-1/2$	N(1B)–H(1B1)–Cl(7)	167(5)
No 10 $-x+1/2, y, z+1/2$	No 10 $x, y-1, z$	N(1B)–H(1B2)–Cl(8) No 1	158(4)
No 11 $-x+1/2, y, z-1/2$	No 11 $x, -y+3/2, z+1/2$	N(1C)–H(1C1)–Cl(8) No 4	150(9)
No 12 $x, -y+1/2, z+1/2$	No 12 $x, -y+1/2, z+1/2$	N(1D)–H(1D1)–Cl(7)	150(5)
No 13 $-x+1, y+1/2, -z+1/2$	No 13 $x, y+1, z+1/2$	N(1D)–H(1D1)–Cl(7)	150(5)
	No 14 $x-1, y, z$		

dispersion ($\Delta\varepsilon_b \approx 13$ units close to T_c) suggests that ionic reorientation is involved in the polarization as expected from the polarity of piperidinium ions.

In order to estimate parameters of the relaxation process measurements of the complex electric permittivity in a wide frequency range were undertaken. Figures 7(a) and (b) show the temperature dependence of the real and imaginary part of the complex electric permittivity at several frequencies from the range between 75 kHz and 30 MHz. The corresponding frequency dependences of the real and imaginary parts of electric permittivity at several temperatures are given in figures 7(c) and (d). The normalized Cole–Cole diagrams at four temperatures are presented in figure 8. It was found that the dielectric relaxation in the PCAPC crystals is well described by the Cole–Cole relation:

$$\varepsilon^* = \varepsilon_\infty + (\varepsilon_0 - \varepsilon_\infty)/[1 + (\mathrm{i}\omega\tau)^{1-\alpha}] \tag{1}$$

where ε_0 and ε_∞ are the low and high frequency limits of the electric permittivity, respectively, ω is angular frequency, τ is the macroscopic relaxation time, and α is the distribution of relaxation time parameter. The values of ε_0, ε_∞, τ and α were fitted for each temperature independently. The values of relaxation time obtained in this way change in the range 10^{-9}–10^{-6} s between 250 and 200 K. The values of α (0.08–0.16) show that the relaxation deviates from the single relaxation process. The α parameter increases with decreasing temperature.

The activation energy, E_a, was calculated according to the Arrhenius equation:

$$\tau = C\exp(E_a/RT) \tag{2}$$

where C is constant. The Arrhenius relation, $\ln\tau$ against reciprocal temperature, is given in figure 9. The estimated value of the activation energy in the high temperature phase amounts to 34.8 kJ mol^{-1}, whereas for the low temperature phase 32.6 kJ mol^{-1}.

3.4. Birefringence measurements and optical observations

In most crystals the greatest planes of as-grown single crystals of PCAPC are parallel to the a–c-plane. The optical index ellipsoid axis-n_γ-is parallel to the c-axis and it is acute bisectrix of the indicatrix. This indicates that the crystal is optically positive. The n_β axis is parallel to the a-axis of the crystal. At room temperature the linear birefringence value, Δn_{ac} (measured with an Ehringhaus compensator), is equal to 7×10^{-3} and diminishes on cooling.

Below the transition temperature ($T_c = 202$ K) one can observe platelike ferroelastic domains with walls parallel to the orthorhombic (100) and (001) planes (see figure 10). Such

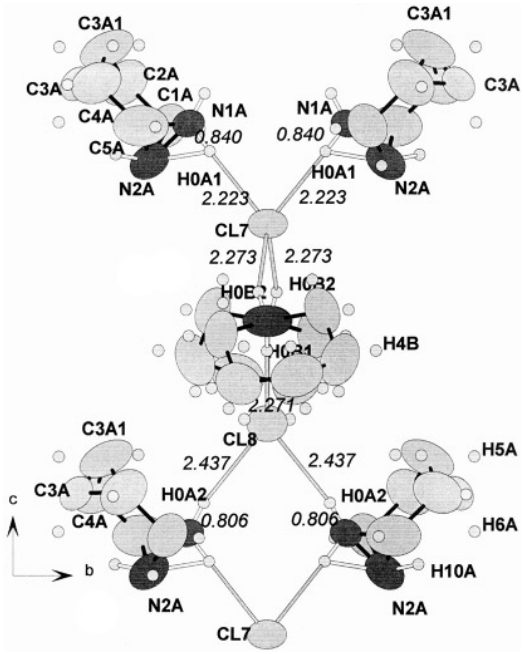

(a)

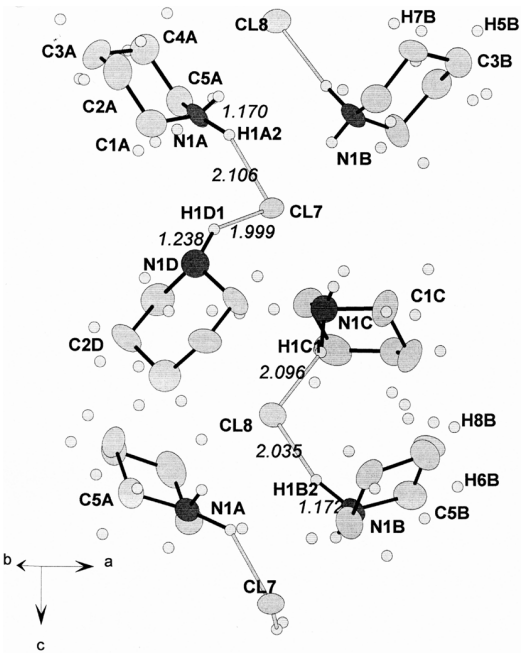

(b)

Figure 3. Hydrogen bond distribution in the PCAPC unit cell: (a) at 293 K, (b) at 185 K.

a domain pattern was expected taking into account the change of the point groups of this crystal from mmm to $2/m$ (according to the Sapriel classification—$mmmF2/m$ species [9]).

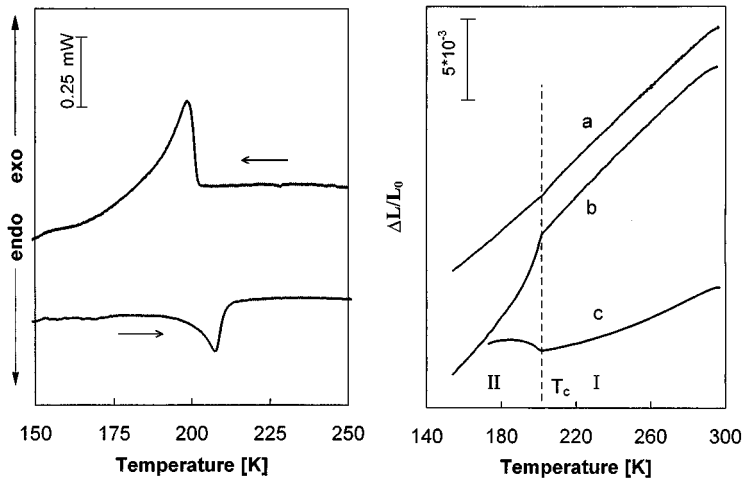

(a) (b)

Figure 4. (a) DSC curves obtained on heating and cooling for PCAPC (scanning rate 5 K min^{-1}; sample mass 15.48 mg). (b) Temperature dependence of the linear thermal expansion $\Delta L/L_0$ of the PCAPC crystal along the *a*-, *b*- and *c*-axes.

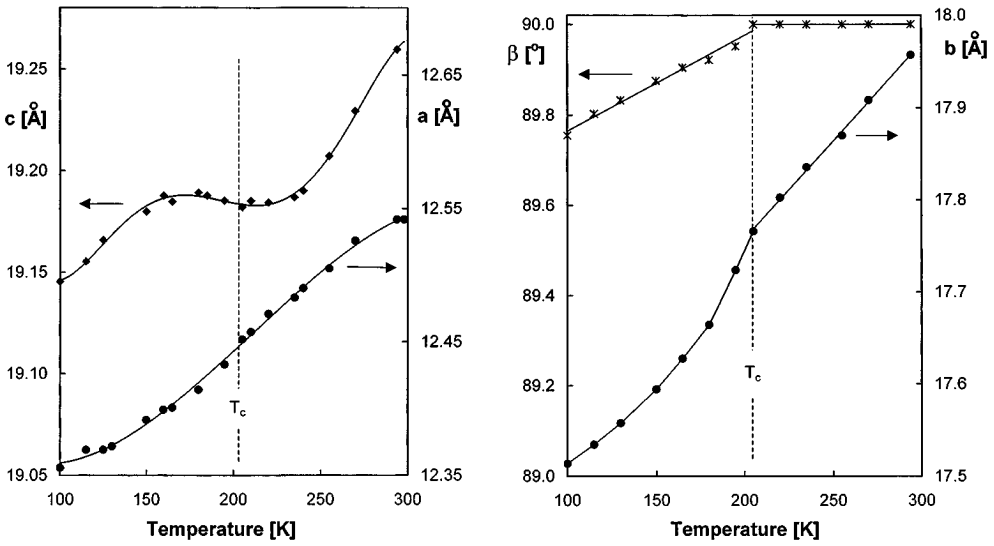

(a) (b)

Figure 5. (a) Experimental values of the lattice parameters *a* and *c* and (b) *b* and the β monoclinic angle as a function of temperature for the PCAPC crystal.

Using the possibility of local measurements of the linear optical birefringence (LB) changes with the rotating analyser method [10] we have performed measurements of the LB changes in the vicinity of the transition temperature along the *b*-axis.

The value of the LB increment, $\delta(\Delta n_{ac})$, was obtained as a difference between the measured changes of Δn_{ac} and the base line extrapolated from the thermal dependence of LB in the paraelastic phase. The temperature dependence of $|\delta(\Delta n_{ac})|$ is shown in figure 11.

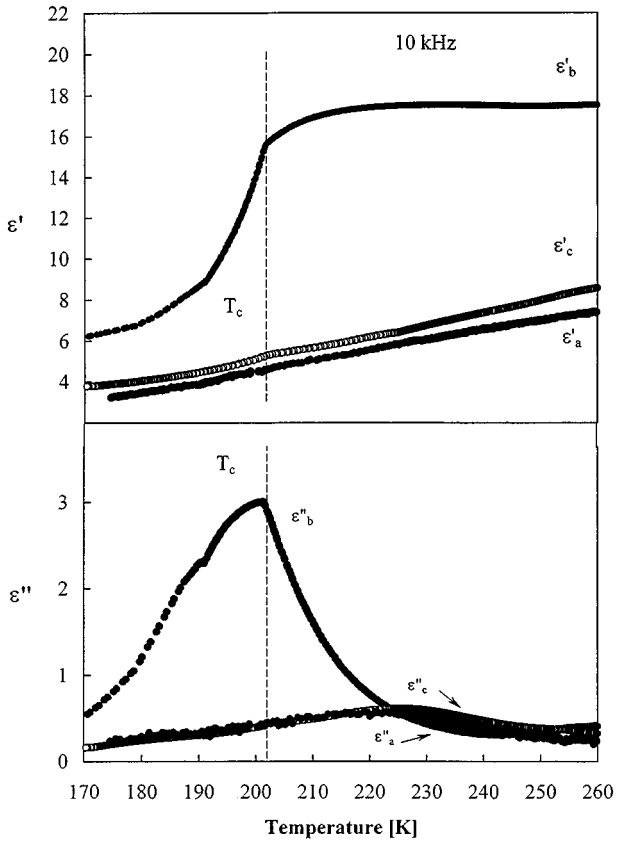

Figure 6. Temperature dependence of the complex electric permittivity, $\varepsilon^* = \varepsilon' - \mathrm{i}\varepsilon''$, measured at 10 kHz along the *a*-, *b*- and *c*-axes of PCAPC.

As shown in figure 11 (inset) the slope of the log–log plots of $|\delta(\Delta n_{ac})|$ against $(T_c - T)$ is equal to 2β ($2\beta \approx 1.0$). The β index was estimated to be 0.5 over the temperature region of about 15 K. It should be noticed that this value changes approaching T_c from below for $T_c - T \approx 0.2$ K.

The increment of LB, Δn_{ac}, should be proportional to the square of the order parameter η [11]. As the increment changes linearly with temperature (see figure 11) one can suggest that the ferroelastic phase transition exhibits the feature of pure second order type.

4. Discussion

DSC and dilatometric studies on PCAPC presented in this paper revealed the presence of a structural phase transition at 202 K. The shape of the thermal anomaly and the lack of temperature hysteresis point out the continuous nature of this transition. In spite of the fact that the phase transition is quite subtle, the relatively large contraction along the *b*- and expansion for the *c*-direction in the vicinity of the phase transition indicate an important change in the structure. From the x-ray measurements it implies that the change is strongly associated with a deformation of the hydrogen bond system. The linear birefringence measurements confirmed the continuous character of the transition at 202 K.

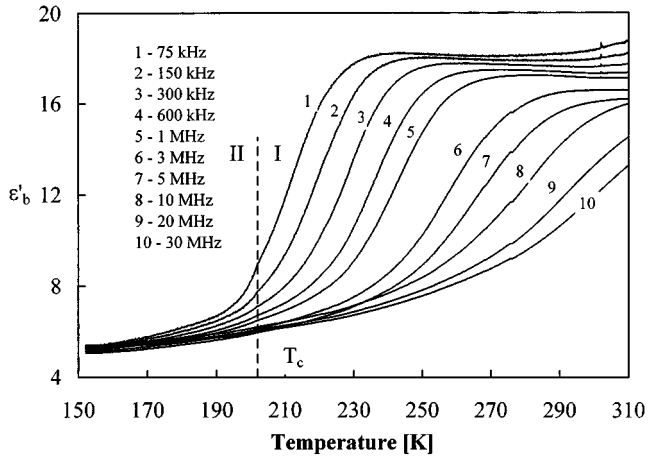

(a)

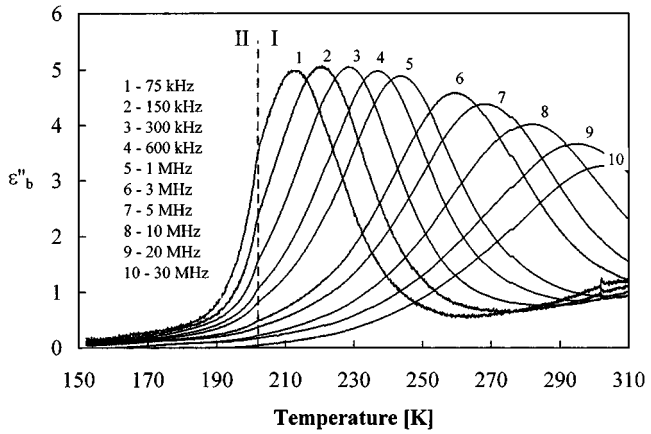

(b)

Figure 7. (a) Temperature dependence of the real and (b) imaginary part of the complex electric permittivity at several frequencies from the range between 75 kHz and 30 MHz for PCAPC. (c) Dielectric dispersion at different temperatures for PCAPC. (d) Dielectric absorption at different temperatures for PCAPC.

The question is, however, open whether we deal with the ferroelasticity below 202 K. X-ray and optical observation show that the phase transition at 202 K creates the lattice distortion, which is connected with it the macroscopic spontaneous strain. It is obvious that the direct confirmation of the ferroelasticity would be the switching of the spontaneous strain by the coercive stress. Regretfully in our case the bad mechanical stability of the single crystals caused that we were unable to perform such an optical experiment. Additionally it was impossible to prepare the samples for elastic measurements due to the small dimensions and pure quality of the single crystal usually obtained from the solution.

Nevertheless we can count the following experimental evidence for PCAPC, which is similar to those observed in typical ferroelastic crystals:

(i) During the phase transition the crystal changes its symmetry from orthorhombic to monoclinic.

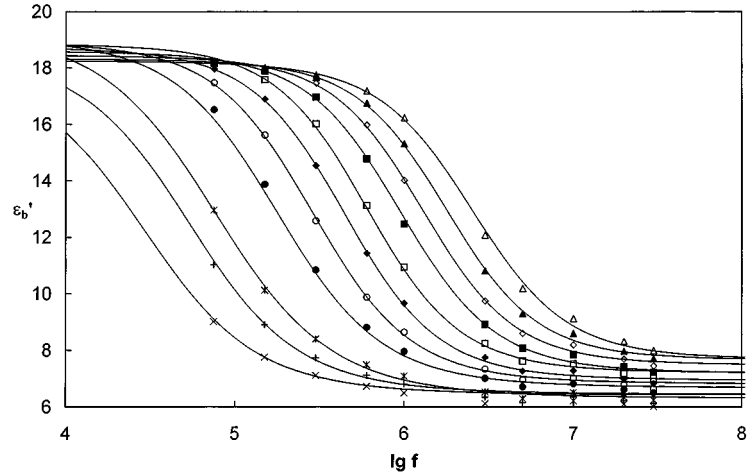

(c)

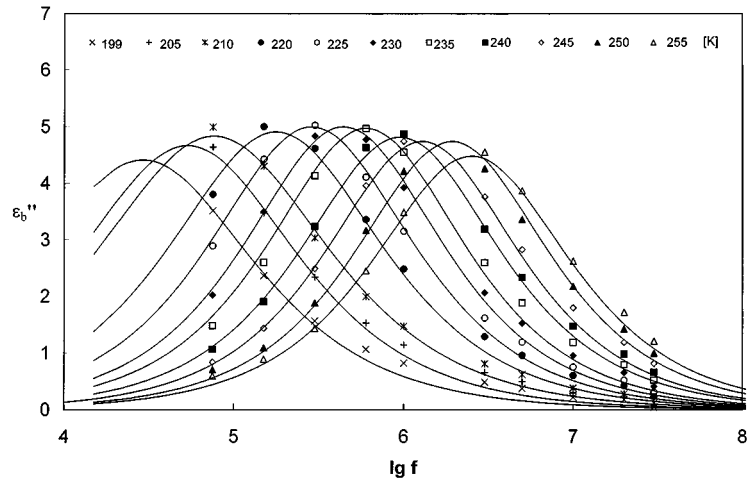

(d)

Figure 7. (Continued)

(ii) Domain-like structure appears exactly below the phase transition point. This effect is clearly reversible with temperature.

(iii) we have observed the characteristic temperature evolution of the monoclinic β angle, which is strictly connected with the spontaneous strain, ε_5^s, being in such a case the order parameter.

Therefore on the basis of the presented structural data and physical properties of PCAPC we can suppose that we really deal with the ferroelastic crystal.

The other question arises about the dynamic or static nature of the orientational disorder of the piperidinium cations in the PCAPC crystals. The structural and dielectric dispersion evidence indicates that the piperidinium orientations are in dynamic disorder in the high temperature phase of PCAPC. Numerous x-ray studies of different ionic piperidinium salts showed that either the puckering between the two chair conformations of the cation (disorder

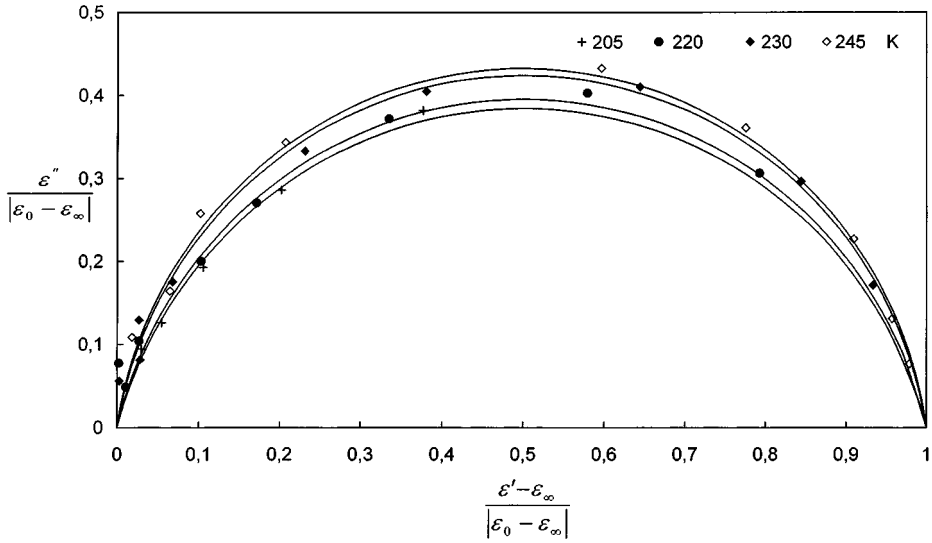

Figure 8. Normalized Cole–Cole diagrams for four temperatures in the high temperature phase of PCAPC.

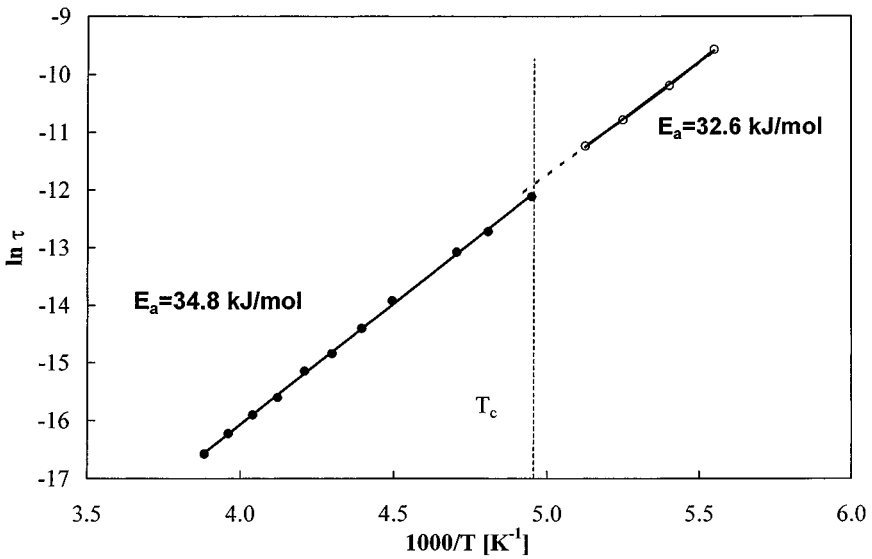

Figure 9. Arrhenius relation, ln τ versus reciprocal temperature, for PCAPC.

of type (a)) or the rotation around the pseudo-C_3 axis of the cation (type b) or the rotation around the C_2 axis of the piperidinium molecule (type (c)) [4] can be considered as typical motional modes. Such an isotropic rotation of the cations was found for example in the highest temperature phases of $(C_5H_{12}N)PF_6$ [4], $(C_5H_{12}N)ClO_4$ [1] and $(C_5H_{12}N)NO_3$ [3] but it is surely not our case. Namely the presented x-ray measurements of PCAPC at 293 K revealed that both N(1A) and C(3A) atoms in one of two independent piperidinium cations possess large thermal parameters. The remaining carbon atoms belonging to this ring (C1A, C2A, C4A and C5A) are described by quite small thermal parameters, so the motional

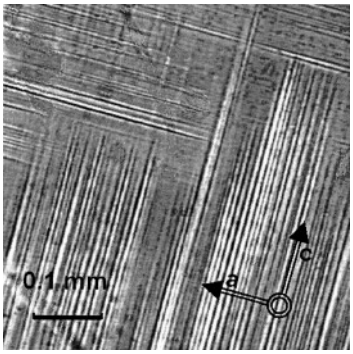

Figure 10. Ferroelastic domain structure in the a–c-plane of the PCAPC crystal at 190 K.

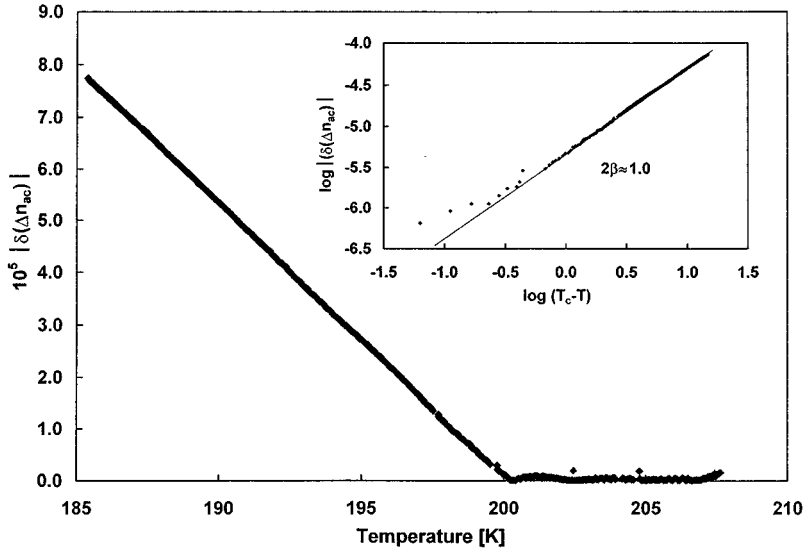

Figure 11. Linear birefringence increment changes in the vicinity of phase transition, on cooling, and the log–log plot of $|\delta(\Delta n_{ac})|$ versus $(T_c - T)$ for PCAPC as an inset.

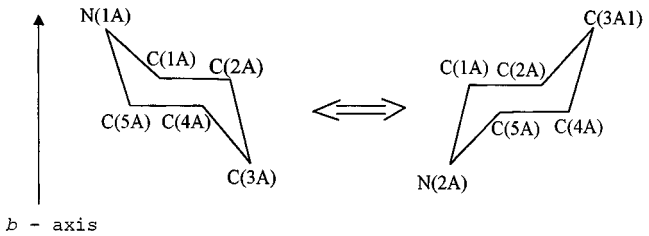

Figure 12. Model of the orientational disorder of the $C_5H_{12}N^+$ cation in the orthorhombic phase of PCAPC.

disorder of type (b) and (c) are undoubtedly excluded. Moreover taking into account the fact that the boat conformation is not present in the ordered low temperature phase of PCAPC it is reasonable to assume that in the high temperature phase we deal with the puckering motion of the piperidinium cation. This may be described by the two-site model of disorder.

The simplified model for such a dynamical disorder of the piperidinium cations (N1A) is illustrated in figure 12.

It is rather difficult to state whether the contribution of the dynamic of the piperidinium cations (N1A) to the mechanism of the phase transition is crucial or whether it is a second order factor. The weak dielectric anomaly around 202 K indicates that the cationic dynamics may change only slightly when the crystal undergoes the phase transition. This supposition is corroborated by nearly the same activation energy estimated above and below 202 K, but the dielectric increment decreases apparently below 202 K. In order to explain the mechanism of the phase transition it is necessary to take into consideration also the other components. The distortion of the crystal lattice accompanying the phase transition may be explained in terms of the change in the hydrogen bond system in both phases. In the high temperature orthorhombic phase the $Cl^-(7)$ and $Cl^-(8)$ ions are symmetrically surrounded by the N atoms, belonging to the disordered piperidinium cations. The hydrogen bonds in this phase are quite weak but they are almost linear. This hydrogen bond system creates a chain along the *c*-axis. In the low temperature phase the significant shortening of some of the hydrogen bonds and the breaking of the others takes place. This results in the appearance of the isolated $C_5H_{10}NH_2^+$–Cl–$C_5H_{10}NH_2^+$ units and the breaking of the chain extending along the *c*-axis. The hydrogen bonds existing in the low temperature phase become slightly non-linear. This is accompanied by a simultaneous shift of the $Cl^-(7)$ ion towards the N(1A) and N(1D) atoms and the $Cl^-(8)$ ion towards the N(1C) and N(1B) atoms. This effect is strictly connected with a continuous diminishing of the flipping motion of the nitrogen atoms with temperature and the ordering of the piperidinium cations.

The proposed model of disordering of dipolar $C_5H_{12}N^+$ cations seems to be well consistent both with the observed anisotropy of the electric permittivity and the existence of the relaxation process. The puckering between two chair conformations gives the largest change of the projection of the dipole moment on the *b*-axis. The studies of the dielectric anisotropy of the PCACA crystal clearly confirm that the largest value of the dielectric increment is really observed along this crystallographic axis. The dielectric relaxation observed at relatively low frequencies indicates that this process is quite slow.

In the high temperature phase it is seen that the dielectric increment $\Delta\varepsilon_b = \varepsilon_0 - \varepsilon_\infty$ and dielectric losses increase on approaching the phase transition point from above (see figure 6). Then in the low temperature phase (below 202 K) we observe the decreasing of $\Delta\varepsilon_b$. There are several factors which may explain such a change of electric permittivity with temperature: (1) increase of density of the crystal, (2) increase of the dipole–dipole interactions and (3) a shape of the potential energy curve describing the dipole reorientation with two non-equivalent minima. Two first factors operate in the same direction enhancing the electric permittivity value. The relatively weak increase of $\Delta\varepsilon_b$ on cooling in the high temperature phase is rather connected with the first effect. On the other hand in the low temperature phase both dielectric increment, $\Delta\varepsilon_b$, and losses distinctly decrease with temperature. Such a behaviour of $\Delta\varepsilon_b$ in this phase we can explain using the Meakins approach [12].

If there is an enthalpy difference, ΔH_0, between the two non-equivalent orientations, the magnitude of the dielectric dispersion is given by the expression:

$$\varepsilon_0 - \varepsilon_\infty = \frac{C}{T}\left(1 + \cosh\frac{\Delta H_0}{RT}\right)^{-1} \tag{3}$$

where C is constant. In this model, when there is an energy difference larger than RT between the two minima, which are separated by the activation energy $E_a = 35\ \mathrm{kJ\ mol^{-1}}$ (see figure 9), the dielectric increment decreases with decreasing temperature. Calculation by fitting the data of the increment in the low temperature phase indicates that the energy difference of the two minima, ΔH_0, is 6 kJ mol^{-1}.

On the other hand also in the high temperature phase the disordering of cations may be described also by potential energy curve with two non-equivalent minima since the occupancy factor for the N(1A) and C(3A) atoms equals 0.61. Nevertheless the dipole–dipole interaction may be dominant in this phase and we should observe as a result the weak increase of ε'_b on cooling. Such a temperature evolution of ε'_b is really observed.

It seems interesting to compare the dielectric properties of the crystal presented in this paper with those of all chlorontimonates(V) studied up to now. In most of the investigated crystals, e.g. $[N(CH_3)_4]SbCl_6$ [7], $[N(C_2H_5)]SbCl_6$ [7] and $[C(NH_2)]SbCl_6$ [6], a small value of electric permittivity was observed ($\sim$10 units and smaller). It was shown that the dynamic of the cations gave the basic contribution to the mechanism of the phase transitions in these salts. Due to the spherical symmetry of the cations their reorientation cannot lead to the important change of the apparent dipole moment in the unit volume.

In the case of PCAPC the high frequency limit value of permittivity (ε_∞) obtained from the Cole–Cole diagrams is equal to about 7 units and this value is comparable to the static electric permittivity of the most of alkylammonium chloroantimonates(V) crystals. The difference in the electric permittivity value from these considerations seems to be quite large ($\Delta\varepsilon \approx 10$ units, see figure 6). That evidences that the dynamic of the non-symmetric piperidinium groups gives the basic contribution to the high electric polarizability of the PCAPC crystal.

5. Conclusions

(1) PCAPC undergoes a second order phase transition at 202 K from orthorhombic symmetry ($Pccn$) to the monoclinic one ($P2_1/n$).
(2) The mechanism of the structural phase transition is due to the disordering of one piperidinium cation N(1A) and the essential change in the N–H . . . Cl hydrogen bond system.
(3) The low frequency relaxator revealed in the high temperature phase of PCAPC is connected with reorientational motion of the dipolar piperidinium groups.
(4) The optical observations by means of polarizing microscopy and x-ray diffraction evidence that PCAPC is a 'potential ferroelastic' crystal below 202 K.

Acknowledgment

This work was supported by the Polish State Committee for Scientific Research (project register 3 T09A 058 17).

References

[1] Ishida H, Ikeda R and Nakamura D 1987 *Bull. Chem. Soc. Japan* **60** 467
[2] Ishida H, Ikeda R and Nakamura D 1982 *Chem. Lett.* **1943**
[3] Ishida H, Ikeda R and Nakamura D 1985 *J. Chem. Soc. Faraday Trans.* II **81** 963
[4] Ono H, Ishimaru S, Ikeda R and Ishida H 1998 *Ber. Bunsenges. Phys. Chem.* **102** 650
[5] Ciapala P, Jakubas R, Bator G, Pietraszko A and Kosturek B 1998 *J. Phys.: Condens. Matter* **10** 5439
[6] Jakubas R, Ciapala P, Pietraszko A, Zaleski J and Kusz J 1998 *J. Phys. Chem. Solids* **59** 1309
[7] Decressain R, Jakubas R, Bator G, Zaleski J, Lefebvre J and Kusz J 1998 *J. Phys. Chem. Solids* **59** 1487
[8] Sheldrick G M 1997 *SHELX_97 Program for the Refinement of Crystal Structures*
[9] Sapriel J 1975 *Phys. Rev.* B **12** 5128
[10] Wood J G and Glazer A M 1979 *J. Appl. Crystallogr.* **13** 217
[11] Fousek J and Petzelt J 1979 *Phys. Status Solidi* a **55** 11
[12] Meakins R J 1960 *Prog. Dielectrics* **2** 153